



PAPER • OPEN ACCESS

# A reproducible extrusion printing process with highly viscous nanoparticle inks

To cite this article: Martin Ungerer *et al* 2024 *Eng. Res. Express* **6** 015042

View the [article online](#) for updates and enhancements.

## You may also like

- [Simultaneous multi-material embedded printing for 3D heterogeneous structures](#)  
Ziqi Gao, Jun Yin, Peng Liu *et al.*
- [Organic Complementary Integrated Circuits Fabricated with Reverse Offset Printed Electrodes](#)  
Yasunori Takeda, Kazuma Hayasaka, Rei Shiwaku *et al.*
- [An open-source bioink database for microextrusion 3D printing](#)  
Bhushan Mahadik, Ryan Margolis, Shannon McLoughlin *et al.*

# Engineering Research Express



## PAPER

# A reproducible extrusion printing process with highly viscous nanoparticle inks

### OPEN ACCESS

RECEIVED  
9 August 2023

REVISED  
15 December 2023

ACCEPTED FOR PUBLICATION  
9 January 2024

PUBLISHED  
18 January 2024

Original content from this work may be used under the terms of the [Creative Commons Attribution 4.0 licence](#).

Any further distribution of this work must maintain attribution to the author(s) and the title of the work, journal citation and DOI.



Martin Ungerer\* , Christian Debatin, Joachim Martel, Volker Maurer, Klaus-Martin Reichert, Andreas Hofmann and Ulrich Gengenbach

Institute for Automation and Applied Informatics (IAI), Karlsruhe Institute of Technology (KIT), Hermann-von-Helmholtz-Platz 1, 76344 Eggenstein-Leopoldshafen, Germany

\* Author to whom any correspondence should be addressed.

E-mail: [martin.ungerer@kit.edu](mailto:martin.ungerer@kit.edu), [christian.debatin@web.de](mailto:christian.debatin@web.de), [martel.joachim@googlemail.com](mailto:martel.joachim@googlemail.com), [volker.maurer@gmx.de](mailto:volker.maurer@gmx.de), [klaus.reichert@kit.edu](mailto:klaus.reichert@kit.edu), [andreas.hofmann@kit.edu](mailto:andreas.hofmann@kit.edu) and [ulrich.gengenbach@kit.edu](mailto:ulrich.gengenbach@kit.edu)

**Keywords:** microfabrication, printed electronics, extrusion printing, fluid-filament printing

## Abstract

Printing of functional materials such as nanoparticle inks is a class of additive fabrication techniques complementary to standard subtractive electronics fabrication techniques such as pcb technology on pcb level or silicon based microelectronics on integrated circuit level. To date the majority of digital printing processes for (micro)electronics is inkjet based. Moreover aerosol jet based printing also establishes itself for printing on non-planar substrates and for materials with higher viscosities. A material deposition technique available since decades and mainly used for dispensing of adhesives and sealing materials is fluid-filament printing. It allows to cover a wide range of materials and viscosities and thus, also holds potential for additive manufacturing of electronics. In this paper we systematically study the influences on fluid filament printing both theoretically taking into account ink and equipment tolerances and experimentally using mainly standard dispensing equipment and two commercial screen printing inks. At the end of the paper we derive recommendations for reproducible printing of conductive lines and pads and give an outlook to printing 2.5D structures.

## 1. Introduction

In important industrial sectors such as Internet of Things (IoT), automotive, consumer electronics, construction, packaging and health care the emerging platform technology Printed Electronics (PE) more and more enables the fabrication of innovative products [1]. In printing processes the materials needed to realize a desired function or electronic element are mostly based on inorganic nanoparticle dispersions, organic solutions or metal organic complexes [2]. In contrast to electronic products fabricated by conventional silicon processes smart devices, wearables, RFID tags, sensors and other products benefit from the versatility of PE by additive, material-efficient and waste-reducing processes on various flexible substrates [1–4].

### 1.1. Printing technologies

Unlike the conventional, printing form based principles, digital printing offers a maximum flexibility in terms of e.g. batch size, choice of substrates, customizability of single products within a lot and enables the set-up of an entirely digital production process chain [2]. Piezoelectric drop on demand (dod) inkjet is one of the most widespread techniques in the field of printed electronics [2, 5–9]. Challenges lie in the combination of the required low viscosity functional inks that are mostly nanoparticle dispersions, appropriate print heads and smooth substrates that do not allow ink penetration [2, 10–12]. Besides piezoelectric inkjet other digital printing principles such as laser induced forward transfer [13, 14], electrohydrodynamic inkjet [15, 16], aerosol jet [17–20] and fluid-filament printing [2] are considered as promising candidates for the fabrication of electronics [21].

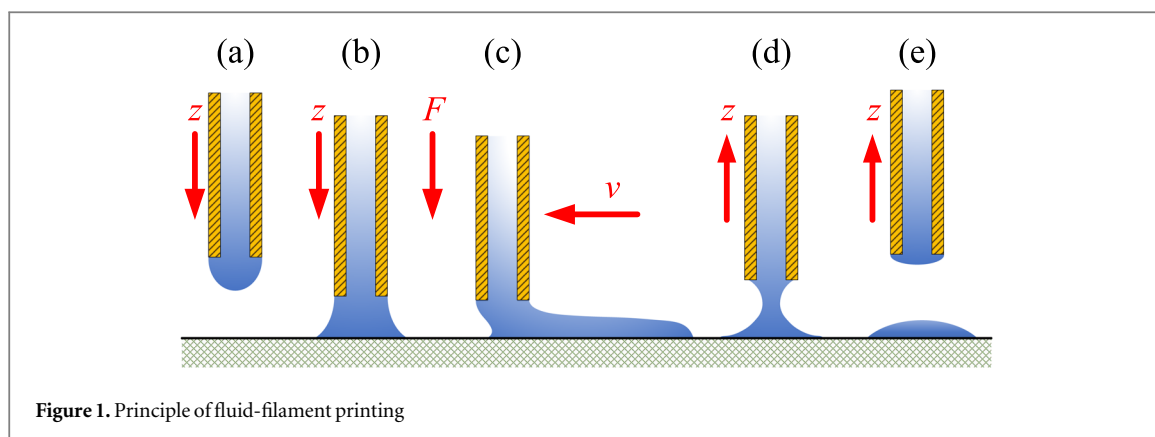


Figure 1. Principle of fluid-filament printing

The class of fluid-filament printing technologies comprises nozzle-based continuous ink printing principles that need a constant fluidic bridge between nozzle and substrate during ink transfer [2]. Figure 1 show the approach (a) of the nozzle until the properly adjusted fluid meniscus comes into contact with the substrate and forms a liquid bridge (b). The ink transfer takes place at a relative motion  $v$  between nozzle and substrate while the ink's massflow is adjusted according to the desired cross section of the liquid filament by the force  $F$  (c). When the ink transfer shall end the ink delivery is stopped and the nozzle is lifted off. In this phase the liquid bridge constricts (d) and breaks shortly afterwards (e).

For reproducible printing the liquid bridge and its shape must be maintained uniform throughout the printing path. Theoretically this can be achieved by control of ink mass flow, relative velocity and standoff distance between nozzle and substrate [2]. This standoff distance has to be kept lower than the inner diameter  $d_i$  of the printing nozzle [22–25]. Particularly for structure widths smaller than a few tens of microns the control of the main printing parameters can be very sophisticated due to increasing influences of substrate topography, surface properties, ink rheology and ambient conditions. Without distance control only very planar and smooth substrates such as glass and silicon wafers can be used for reproducibly printing very small structure widths.

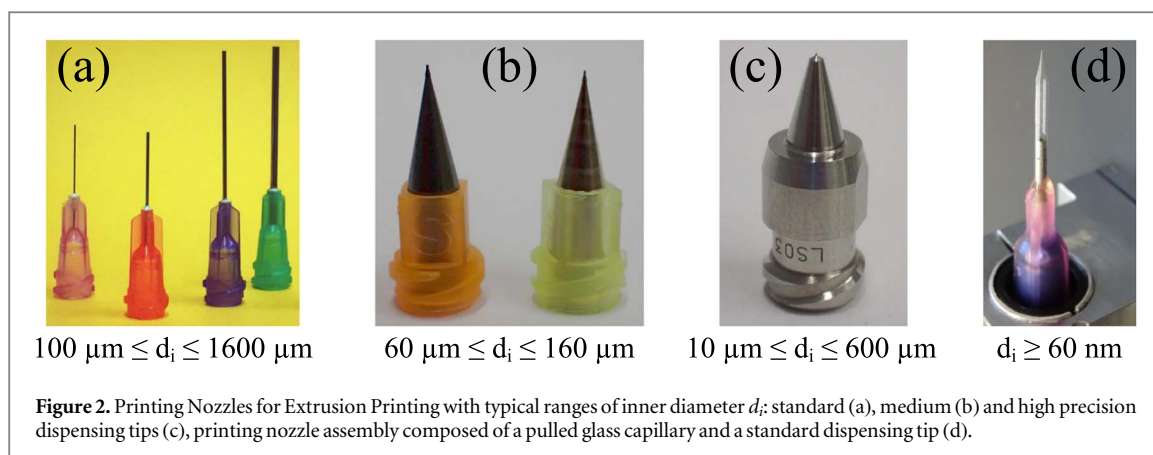
Depending on the method of force application for the ink transfer the fluid filament printing principles can be classified into three groups: ultrasonic plotting [26–28], capillary driven [25] and extrusion printing [29–31]. In contrast to all other printing technologies, fluid-filament printing enables the broadest range of ink viscosities.

Inks with very low viscosities can be printed without application of an external force for ink transfer by surface force driven capillary printing (CP) [25]. Ultrasonic plotting (UP) provides a fluid pumping force actuated by ultrasonic vibrations of the nozzle and thus, permits a broader viscosity range (up to 450 mPa s) [32, 33]. Extrusion printing (EP), often referred to as direct ink writing [34] or omnidirectional printing [35] can be adapted to very high ink viscosities (from about 1 mPa s to  $10^6$  mPa s) [24] and is the most important fluid-filament printing technology applied in printed electronics. 3D structures made from ceramics [34] or polyelectrolyte complexes [36], spanning and flexible microelectrodes as alternative to wire bonding [35], conducting tracks having structure widths in the lower mm range onto photo paper [31], liquid metal resistors and interconnects [29] have been reported. To ensure ink transfer EP needs an external pressure that can be applied via established dispensing technologies such as the rotary screw, positive displacement (piston) and time-pressure method [31, 37–39].

## 1.2. Motivation

Additive manufacturing of structures with widths in the range of tens of microns and lower both in 2D and 3D as well as spanning electrodes providing low electrical resistances are of great interest for electronics applications such as interconnects, wire-bonds, antennas, transparent electrode grids, resistors, diodes, transistors and sensors, e.g. for wearable and biomedical systems [29, 35, 40–43].

The main challenges set out in the state of the art are reproducible printing of highly conductive structures with lengths  $\gg 10$  mm and widths down to the single micrometer range both on 2D and on non-planar, 3D substrates using commercially available materials. Companies such as NScrypt (USA), KELENN Technology (France) or XTPL (Poland) offer solutions for high resolution EP based electronics fabrication [44]. SonoPlot (USA) and Hummink (France) provide UP equipment. These companies are currently promoting their technologies for applications such as RFID tags, biosensors, batteries, photovoltaics, miniaturisation of PCBs, via filling, open defect repair of TFTs in displays, dispensing of optoelectronic polymers e.g. for fabricating optical waveguides, precise deposition of quantum dots and DNA solution microarrays. However the offered solutions are based on proprietary dispensing equipment and inks.



Our objectives are to meet the above challenges, by systematically investigating the parameters influencing the EP process and by printing highly conductive planar test tracks as well as showing a perspective to print 2.5/3D structures. We validate this approach by a modular inhouse developed vector-based printing system composed of off the shelf components such as axis modules, motion control, dispensing system, dispensing nozzles and nozzles fabricated inhouse from glass capillaries. In contrast to the above approaches we use commercially available screen printing inks to evaluate both reproducibility of the printed structures and process stability with regard to general applicability.

The paper is structured as follows: section 2 introduces materials and methods in particular commercial and inhouse fabricated glass printing nozzles, inks and substrates and the inhouse built printing system. Moreover the theoretical and experimental investigations for identifying EP process parameters and parameter windows are covered. Section 3 presents optical and electrical characterisation results of printing test structures with different inks, nozzles and process parameters. Section 4 discusses the experimental results and gives recommendations on the selection of nozzle, ink and process parameters. Section 5 concludes with an outlook how the extrusion process can be further improved towards reproducible printing of even finer structures and towards its extension to 2.5D structures.

## 2. Materials and methods

In this section the printing nozzles, the inks and the experimental setup to realise the EP process are described. Furthermore the processes for printing planar test structures are depicted followed by the characterization methods applied.

### 2.1. Printing nozzles

The connection interface between printing nozzles and the standard dispensing cartridge of the print head is a luer lock connector. There are various commercially available dispensing nozzle types with luer lock that in general can also be used for EP. As depicted in figure 2 these can be subdivided into commercial standard (a), medium (b) and high precision dispensing tips (c). Furthermore glass capillaries mounted onto standard dispensing needles (e.g. Fisnar 8 001 076) can be used as printing nozzles (d).

By means of a micropipette puller glass capillaries with very small tip diameters  $\leq 1 \mu\text{m}$  from commercially available glass tubes (e.g. Hilgenberg borosilicate glass capillaries 1 409 036) can be fabricated. For larger tip diameters well controlled breaking is required [2].

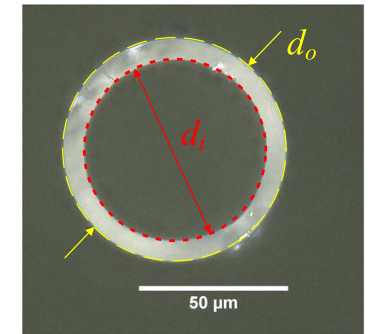
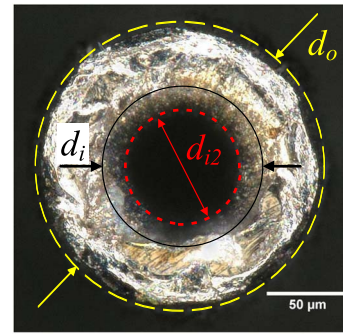
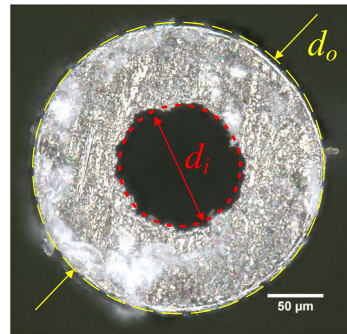
For the present investigation we select the smallest available standard dispensing tip from Vieweg (F561387-1/4), the smallest available medium precision dispensing tip from Subrex (A-100-03-00-02-1) and self-produced glass nozzles that are individually selected due to larger diameter variations caused by the low reproducible tip breaking process. From each nozzle type we analyze the orifices of a few specimen by means of a Keyence light microscope and stacked focus images. The results are summarized in table 1 whereby the customized glass capillaries are provided from BioMedical Instruments.

As can be seen from table 1, Vieweg F561387-1/4 and Subrex A-100-03-00-02-1  $d_i$  have both higher standard deviations compared to commercial glass capillaries. The end face of the metal-based tips show much higher roughness and a much lower dimensional accuracy (high cylindricity deviations) in contrast to the glass nozzles that provide very smooth surfaces and well defined edges (cf microscope images in table 1). Especially for most of the Subrex tips the nozzle exit plane is not clearly defined. The image and 3D measurements show that the orifice is rather blunt and  $d_i$  is difficult to determine exactly. Based on the microscopic analysis and 3D information of

**Table 1.** Measured inner and outer diameters ( $d_i$  and  $d_o$ ) of different printing nozzles. Results are given as *mean ± standard deviation*.

Nozzle type	Standard dispensing tip Vieweg F561387-1/4	Medium precision tip Subrex A-100-03-00-02-1	Glass capillary
sample size	19 <sup>a</sup>	3	9
$d_{i,nominal}$ in $\mu\text{m}$	110	57	60
$d_i^b$ in $\mu\text{m}$	$112.3 \pm 4.4$	$96.9 \pm 2.7$	$60.6 \pm 0.7$
$d_{i2}^c$ in $\mu\text{m}$	—	$69.8 \pm 1.3$	—
$d_{o,nominal}$ in $\mu\text{m}$	310	169	—
$d_o$ in $\mu\text{m}$	$251.9 \pm 5.0$	$172.6 \pm 0.6$	$73.7 \pm 0.8$

Microscopic stacked focus image of the nozzle orifice



<sup>a</sup> thereof 10 from batch #a and 9 of batch #b.

<sup>b</sup>  $d_i$  measured in the nozzle exit plane.

<sup>c</sup> smallest  $d_i$ , measured about 30  $\mu\text{m}$  back from nozzle exit plane.

**Table 2.** Inks used and ink data as provided by the supplier.

Ink/batch #	Viscosity (at 25 °C) in Pa s @ s <sup>-1</sup>	Metal content in wt-%	Particle type/size
Harima NPS <sup>a</sup>	100 @ 1	83	Ag NP/8 nm to 15 nm
Harima NPS #1	72.7 <sup>b</sup> @ 1	80.4	with a mean diameter
Harima NPS #2	107.1 <sup>b</sup> @ 1	82.3	of 12 nm
Dyesol DYAG50 <sup>a</sup>	13-17 @ 10	75-85	metal organic complexes and Ag flakes <sup>c</sup>
Dyesol DYAG50 #1	13.5 @ 10	83.7	

<sup>a</sup> nominal values.

<sup>b</sup> measured by means of a spiral viscometer.

<sup>c</sup> particle size is not disclosed by the manufacturer Greatcell Solar Materials Pty Ltd.

the stacked focus images a  $d_i$  in the nozzle plane is determined as well as a  $d_{i2}$ , measured at about 30  $\mu\text{m}$  back from the nozzle exit plane. In contrast to  $d_i$  the  $d_{i2}$  represents much more the inner diameter of the nozzle's cylindrical section and is thus the more relevant parameter for the dispensing process.

## 2.2. Inks and substrates

Ahn *et al* found that high viscosity inks enable printing of highly conductive, high aspect ratio and even spanning structures without any supporting material [35, 41, 45]. Based on these findings we select the thixotropic silver nanoparticle (NP) based screen printing paste NPS from Harima. The two batches we have been delivered have different viscosities and metal content as laid down in the certificate of analysis (see table 2). For the batch #2 we verify the rheological properties with own measurements (plate/plate rheometry) and find a mean viscosity of about 510 Pa s at a shear rate of 5 s<sup>-1</sup>, 303 Pa s at 10.8 s<sup>-1</sup> and 44 Pa s at 50.2 s<sup>-1</sup>. This confirms a shear thinning behaviour. Moreover we chose the Dyesol DYAG50 (Sigma-Aldrich 791 873) silver particle/metal organic complex ink. The material data of these inks are summarized in table 2.

After printing the silver inks are dried, cured and sintered in a Memmert UP 500 oven. The Harima NPS ink is sintered for 60 min at 220 °C, the maximum temperature of the oven and thus 10 K below the 230 °C recommended by the ink manufacturer. The Dyesol DYAG50 is sintered for 8 min at 180 °C as recommended by the ink manufacturer.

Standard microscope glass slides as well as polyimide films with a thickness of  $t_f = 125 \mu\text{m}$  (Kapton HN Goodfellow 667-985-89) are used as substrates for printing planar test structures.

## 2.3. Extrusion printing system

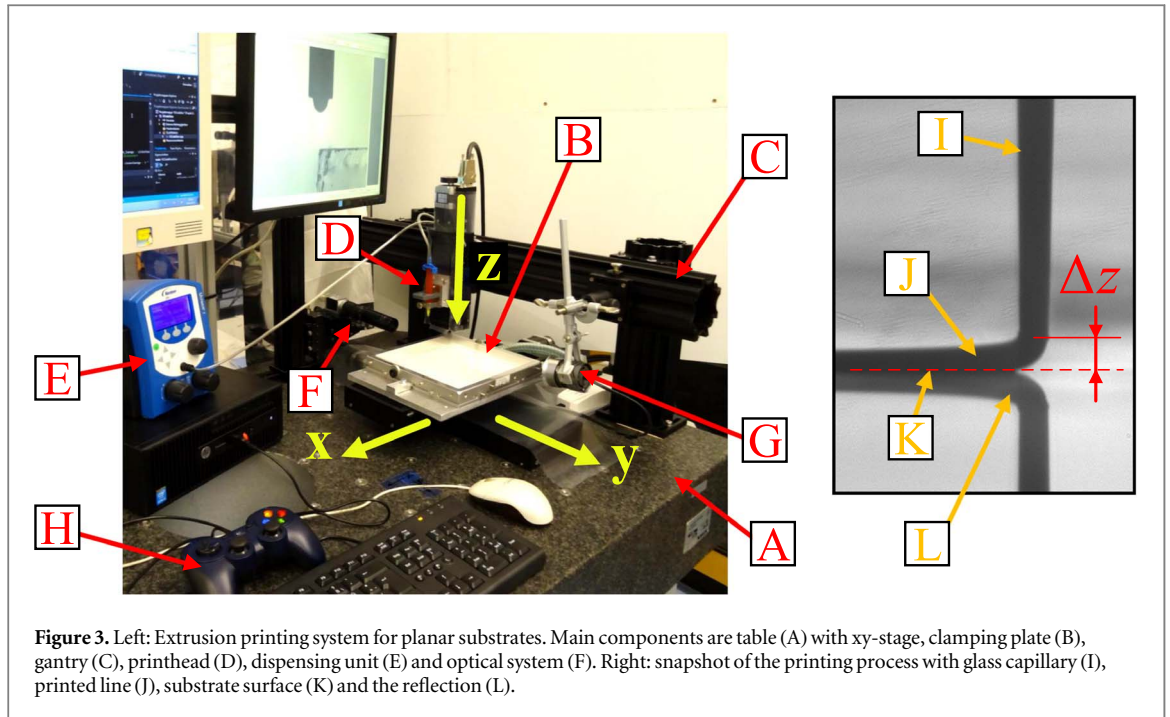
We set up a highly flexible, modular EP system that can be easily adapted to different applications not only for planar but also for curved and 3D substrates.

Figure 3 shows the configuration for printing onto planar substrates and polymer films on the left. On a granite table (A) a xy-stage with a microporous vacuum clamping plate (B) (Witte Barskamp) with a flatness of less than 5  $\mu\text{m}$  is mounted. Moreover the printing system encompasses a gantry (C) (Owis S 65-4 profiles) supporting the z-axis with the print head (D), a Nordson Ultimius I time-pressure dispensing unit (E), an optical system (F), a LED illumination (G), a Logitech F310 Joystick (H) as user interface and a Beckhoff PLC control system.

The xy-stage is composed of two crosswise mounted high-precision stepper motor and ball-screw driven linear stages Owis LIMES 122-160-HSM with recirculating ball bearing guides and Hall-effect limit switches providing a travel of 155 mm, a max. velocity of 25 mm s<sup>-1</sup> and a bidirectional repeatability of less than 2  $\mu\text{m}$ . As z-axis an Owis LIMES 60-70-HSM of the same stage type is used providing a travel of 70 mm, a max. velocity of 30 mm s<sup>-1</sup>. The print head is composed of a Nordson 3 cm<sup>3</sup> syringe barrel that is fixed on the z-axis via a magnetic clamping setup, a printing nozzle and a Nordson syringe barrel adapter that connects the cartridge to the Ultimius I dispensing unit. The optical system comprises a Basler ac1600-20gm monochrome GigE camera and a Navitar Precise Eye (1-61456 with 1-61450) 2x fixed-focus lens with a C-mount adapter and extension tubes of in total 35 mm length in order to get a magnification of 3.6. Together with the LED illumination it is used for manual control of the distance between nozzle and substrate. On the right in figure 3 a snapshot of the printing process is depicted, captured by means of the optical system for the control of  $\Delta z$ .

## 2.4. Theoretical investigation of printing parameters and their influences

EP is based on a well defined, continuous flow of the ink through the nozzle. Hence, it can be regarded as a tube flow as described by the Hagen-Poiseuille law with the volumetric flow rate  $\dot{V}$ , the inner diameter of a straight, cylindrical capillary  $d_{ci}$ , the dynamic viscosity  $\eta$  and the pressure drop  $\Delta p$  between both ends of the capillary of



**Figure 3.** Left: Extrusion printing system for planar substrates. Main components are table (A) with xy-stage, clamping plate (B), gantry (C), printhead (D), dispensing unit (E) and optical system (F). Right: snapshot of the printing process with glass capillary (I), printed line (J), substrate surface (K) and the reflection (L).

the length  $l_c$ :

$$\dot{V} = \frac{\pi d_{ci}^4 \Delta p}{128 \eta l_c} \quad (1)$$

The Hagen-Poiseuille equation (see equation (1)) can be derived from the Navier–Stokes equations, neglecting inertial forces and assuming a laminar, fully developed, steady flow of an incompressible, Newtonian fluid with a maximum velocity of flow on the tube’s axis and wall adhesion. Despite some simplifications (cf. in particular the assumption of a Newtonian fluid) and non cylindrical, more complex inner shapes of dispensing tips and nozzles (cf table 1), equation (1) can be used to discuss the influence of the respective ink and nozzle parameters.

The viscosity of the ink has a linear influence on the pressure drop at a certain volumetric flow rate. For example the viscosity difference between batch #1 and #2 of Harima NPS (see table 2) leads to a pressure drop variation of about 32.1 % related to batch #2. The same linear influence has the length of the cylindrical capillary. A significant influence, with the power of four, has the inner diameter  $d_{ci}$ . Assuming an ink is to be extruded at a given volumetric flow rate through a cylindrical Vieweg F561387-1/4 dispensing tip the variance of the tips characterised and used  $d_{ci} = d_i$  (see table 1) leads to a pressure drop variation of about 24.9 %. The same calculation with the tolerance of the small cylindrical nozzle part of the Subrex A-100-03-00-02-1 yields a pressure drop variation of 73.1 %. In order to achieve the desired ink flow rate a forward pressure must be applied at the dispensing tip. In our set-up this pressure is controlled by the Nordson Ultimius I dispenser controller. This instrument has a pressure tolerance of  $\pm 2\%$  specified by the manufacturer. Eventually, the compressibility of the air inside the cartridge and the tubing has to be considered especially during switching operation of the dispenser valve.

The depicted theoretical considerations indicate that ink property tolerances, nozzle and instrument tolerances have to be taken into account to establish process windows for reproducible printing.

## 2.5. Experimental investigation of printing parameters and their influences

Printing parameters and their influences on structure morphology are investigated by printing straight lines onto microscopy glass slides. In first tests a Vieweg F561387-1/4 standard steel dispensing tip with a measured  $d_i = 119.7 \mu\text{m}$  is investigated. The highest fluid pressure supplied by the pressure controller ( $p = 6.4 \text{ bar}$ ) is required to extrude ink (Harima NPS batch #2) through this type of dispensing tips. The distance between nozzle and substrate is initially adjusted to  $\Delta z = 75 \mu\text{m}$  to achieve a good ink transfer to the substrate. With this parameter set lines with a length of several tens of millimeters are printed at a first velocity setting of  $v_p = 100 \text{ mm min}^{-1}$ . As the fluid filament breaks up regularly and therefore only dotted lines can be printed the velocity is reduced. At  $30 \text{ mm min}^{-1}$  continuous and smooth lines form. In further tests the parameter  $\Delta z$  is varied in order to investigate its influence on the printing process and to find appropriate values for reproducible printing. For this purpose parallel, 10 mm long, meandering lines are printed with all the other parameters kept constant while  $\Delta z$  is varied from line to line from  $35 \mu\text{m}$  to  $225 \mu\text{m}$  in steps of  $10 \mu\text{m}$ . After sintering a

**Table 3.** Process parameters and parameter windows for printing lines (linewidth  $w_l$ ) and pads with different inks and nozzles onto glass substrates.

Nozzle type	Ink	$d_i$ in $\mu\text{m}$	$p$ in bar	$\Delta z$ in $\mu\text{m}$	$v_p$ in $\text{mm min}^{-1}$	$\Delta y$ in $\mu\text{m}$	$w_l$ in $\mu\text{m}$
Vieweg F561387-1/4	Harima NPS	119.7	6.0–6.4	45–55	30	72–80	95–156
Vieweg F561387-1/4	Dyesol DYAG50	115.6	1.2–1.4	45	102–120	120–130	231–272
Subrex A-100-03-00-02-1	Harima NPS	$100.0 \pm 5.1^a$	0.9–1.2	40–60	33–240	—	72–247
Glass nozzle <sup>b</sup>	Harima NPS	41.6	4.3	33	120	—	36.8
		36.6	6.3	25	48	30	55–57
		33.2	6.2	27	120	—	23.6
		31.9	6.5	25	48	30	40–44
		16.9	6.1	10	18	—	12.5
Glass nozzle	Dyesol DYAG50	34.6	0.77	25	60	30	148

<sup>a</sup> Mean  $\pm$  standard deviation of five nozzles with  $d_i$  between 94  $\mu\text{m}$  and 106  $\mu\text{m}$ .

<sup>b</sup> Parameters for selected glass nozzles.

microscopic analysis shows that the line breaks up from  $\Delta z \geq 135 \mu\text{m}$ . Around the meander turns breakup occurs already from  $\Delta z \geq 95 \mu\text{m}$ . Confocal profile measurements show that for  $\Delta z = 35 \mu\text{m}$  the resulting line is flattened. The results of repeated printing tests confirm the conclusion that for a standoff distance of  $40 \mu\text{m} \leq \Delta z \leq 80 \mu\text{m}$  reproducible printing of lines is possible. The best results with respect to a small, homogeneous line width and a smooth edge quality can be achieved for  $45 \mu\text{m} \leq \Delta z \leq 55 \mu\text{m}$ . For a given pressure and a  $\Delta z$  in the favorable process window printing speed, i.e. relative velocity between nozzle and substrate, is the only parameter that influences the cross section of the printed lines.

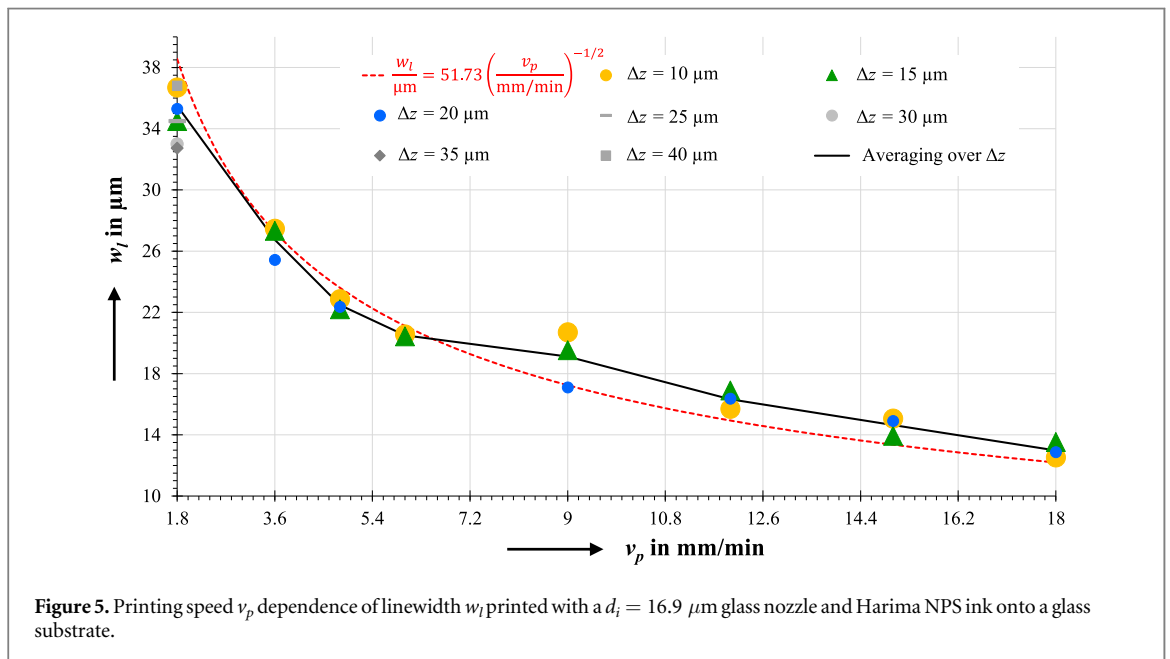
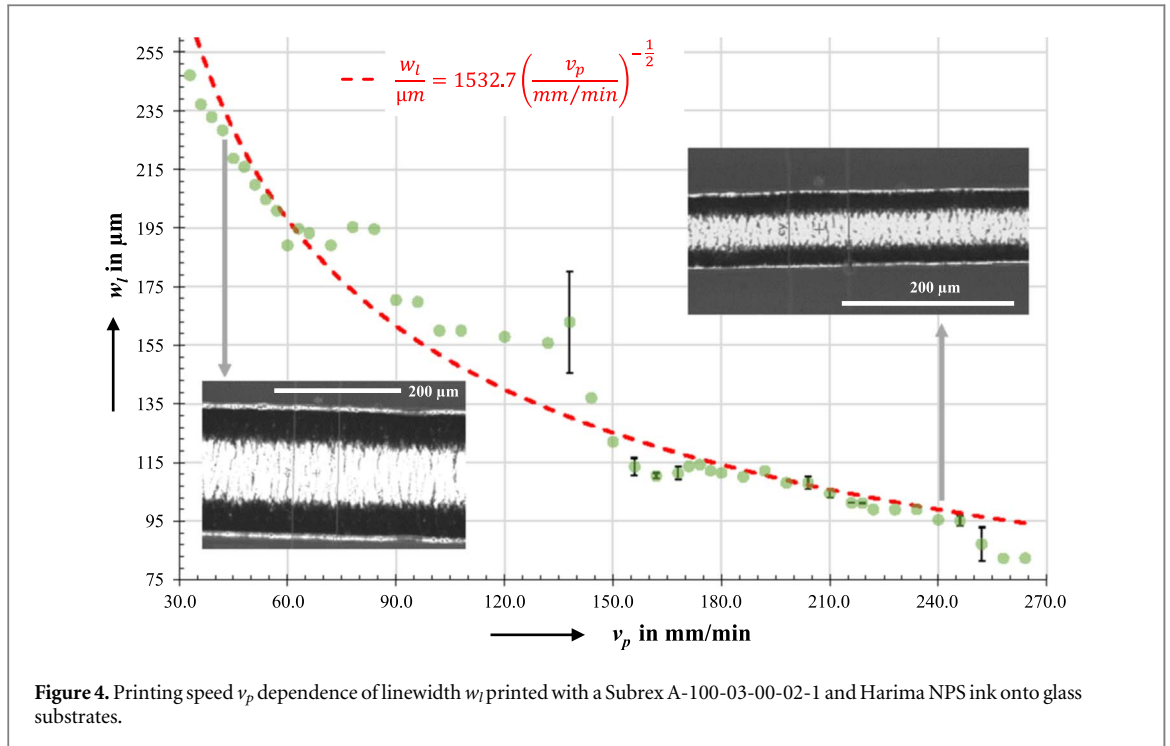
If the ratio flow rate/printing speed is too high the fluid filament will be compressed resulting in wider lines that tend to bulge. Too low flow rate/printing speed ratios lead to a stretched fluid filament and as a consequence to smaller lines that can break up. Between bulging to breakup the ink rheology and the surface properties of the substrate determine the behaviour of the fluid filament.

With the same nozzle type and ink pads can be realized by printing meanders with overlapping lines. Ideally the pitch  $\Delta y$  between neighbouring lines is selected in such a way that they overlap and coalesce to form a homogeneous surface with a smooth cross-sectional profile. Printing experiments show that with all other parameters set as above for  $72 \mu\text{m} \leq \Delta y \leq 80 \mu\text{m}$  homogeneous pads can be printed.

The same methodology has been applied for other combinations of inks, nozzles and substrates. The main process parameters are summed up in table 3. While parameter windows are given for the metal needles, parameter sets are shown for selected glass nozzles exemplarily. The ink and nozzle property influences derived above from the Hagen-Poiseuille equation are reflected in these data. Compared to Harima NPS, the Dyesol DYAG50 shows a significantly stronger spreading on the glass substrate. Accordingly a larger  $\Delta y$  for printing smooth pads can be used.

The printing parameter ranges for specific ink nozzle combinations can be favourably applied to adjust the printed line width over a wide range by means of printing speed variation. Figure 4 shows the line width printed with Harima NPS and a Subrex A-100-03-00-02-1 onto glass for  $33 \text{ mm min}^{-1} \leq v_p \leq 264 \text{ mm min}^{-1}$ . It can be seen that line width  $w_l$  decreases proportionally to the reciprocal of the root of the path velocity  $v_p$ . The correlation  $w_l/\mu\text{m} = 1532.7(v_p/\text{mm min}^{-1})^{-1/2}$  (dashed line in figure 4) is approximated by the least squares method and possesses a coefficient of determination of  $R_B^2 = 0.95$ . For  $\Delta z = 50 \mu\text{m}$ ,  $p = 1.0 \text{ bar}$  and  $v = 180 \text{ mm min}^{-1}$  20 lines of the length 55 mm are printed. The resulting mean width of  $80.0 \mu\text{m}$  with a standard deviation of  $3.8 \mu\text{m}$  and zero rejects demonstrate the high reproducibility of the printing process.

Very narrow lines can be printed with glass capillaries. The process parameters are established with the same methodology as above. Also here line width  $w_l$  decreases proportionally to the reciprocal of the root of the path velocity  $v_p$ . This is illustrated in figure 5 for different values of the standoff distance  $\Delta z$ . Here, the standard deviation of the width of each line is less than or equal to  $0.5 \mu\text{m}$ . For nozzles with  $d_i$  in the range of about  $32 \mu\text{m}$  to  $37 \mu\text{m}$  optimum line distance for printing pads are found to be  $\Delta y = 30 \mu\text{m}$ . Based on measurements by means of a laser scanning microscope correlations of the cross sectional area  $a_l$  with  $a_l/\mu\text{m}^2 = 156.08(v_p/\text{mm min}^{-1})^{-1}$ , the line width  $w_l$  with  $w_l/\mu\text{m}^2 = 51, 73(v_p/\text{mm min}^{-1})^{-1/2}$  and the line height  $h_l$  with  $h_l/\mu\text{m} = 5.37(v_p/\text{mm min}^{-1})^{-1/2}$  related to the printing speed  $v_p$  can be found. In all cases the coefficient of determination is  $R_B^2 \geq 0.94$ . For  $\Delta z = 22 \mu\text{m}$ ,  $p = 2.7 \text{ bar}$  and  $v = 12 \text{ mm min}^{-1}$  60 lines of the length  $15 \mu\text{m}$  to  $20 \mu\text{m}$  are printed using two different glass nozzles each with  $d_i = 29.1 \mu\text{m}$ . The resulting



mean width of  $26.9 \mu\text{m}$  with a standard deviation of  $1.6 \mu\text{m}$  again demonstrates the high reproducibility of the printing process.

For the combination of nozzles with small  $d_i$  and substrates without high planarity it is challenging to print reproducibly for low values of  $\Delta z$  without closed loop control. The ideal standoff distance  $\Delta z$  for dispensing depends on parameters such as ink rheology and nozzle geometry and must usually be determined prior to the printing process [38]. In standard dispensing processes such as adhesive or solder dispensing a standoff distance/nozzle diameter ratio of about  $0.5 \leq \frac{\Delta z}{d_i} \leq 0.7$  is recommended [46–50].

For the tested standard dispensing tips in combination with NPS  $\frac{\Delta z}{d_i} = 0.39$  lead to optimum printing results. For medium precision nozzles with  $0.38 < \frac{\Delta z}{d_i} < 0.58$  and for glass capillaries with  $0.59 < \frac{\Delta z}{d_i} < 0.80$  a broader range is found. In the special case of line printing without changes in direction even  $\frac{\Delta z}{d_i} = 2.37$  is feasible for small glass capillaries. Such large standoff distances are very favourable for printing with small inner

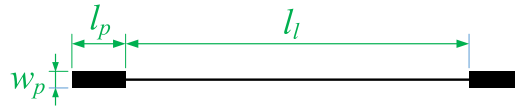


Figure 6. Schematic of the planar test structure.

Table 4. Selected process parameters for printing the planar test structure with different inks, nozzle types and specimens onto glass and polyimide substrates.

Nozzle		ink	$d_i$ in $\mu\text{m}$	p in bar	$\Delta z$ in $\mu\text{m}$	$v_p$ in $\text{mmmin}^{-1}$	$\Delta y$ in $\mu\text{m}$
Type	# <sup>a</sup>						
Vieweg F561387-1/4	S1	Harima NPS	116.4	6.4	45	18	78
	S2	Dyesol DYAG50	115.6	1.4	45	120	130
Glass nozzle	G1-G5	Harima NPS	$34.8 \pm 1.9^b$	6.4	25	48	30
	G6	Dyesol DYAG50 <sup>c</sup>	34.6	0.77	25	60	30

<sup>a</sup> Specimen.

<sup>b</sup> Mean  $\pm$  standard deviation of  $d_i$  with: G1: 31.9  $\mu\text{m}$ , G2: 33.6  $\mu\text{m}$ , G3: 35.2  $\mu\text{m}$ , G4: 36.6  $\mu\text{m}$ , G5: 36.8  $\mu\text{m}$ .

<sup>c</sup> DYAG50 in combination with glass nozzle is only tested on glass substrate.

tip diameters  $d_i$  onto not perfectly planar substrates without closed loop control of the standoff distance  $\Delta z$ . In contrast, the XTPL printing system is working with  $d_i \leq 10 \mu\text{m}$ ,  $\Delta z$  from 0  $\mu\text{m}$  (contact) up to tens of micrometers and  $v_p \leq 60 \text{ mm min}^{-1}$ , preferably when the nozzle is tilted with an angle of  $50^\circ$  to  $60^\circ$  to the substrate [44]. In this case the tilting direction determines the printing direction.

Glass capillaries as nozzles for printing DYAG50 onto glass substrates allow relatively high printing velocities at a comparably low pressure. Up to 600  $\text{mm min}^{-1}$  are tested with an obliquely broken glass nozzle at 3.3 bar and  $\Delta z = 30 \mu\text{m}$ . Due to the DYAG50 particle size, printing with small  $d_i$  is not reliable as nozzle clogging occurs rapidly after process start. Nevertheless, if clogging can be avoided, the quality of the printed results with respect to a homogeneous line width and a smooth edge is very high.

Even though the ratio  $\frac{\Delta z}{d_i}$  for DYAG50 is similar to that for NPS in the case of standard dispensing tips and glass capillaries, other parameters such as the interaction with the substrate surface are different due to different rheological properties. DYAG50 shows a spreading on the substrate right after ink transfer that leads to a more homogeneous pad surface and allows wider line spacings and thus a much lower pad fabrication time. In contrast NPS shows almost no spreading on the substrate. This property of NPS allows printing of the narrowest lines, but on the other hand leads to problems printing pads. In conclusion, it can be said that optimal results in terms of printing resolution, speed and quality can be obtained by combining Harima NPS for printing narrow lines and Dyesol DYAG50 for printing larger pads with a smooth surface.

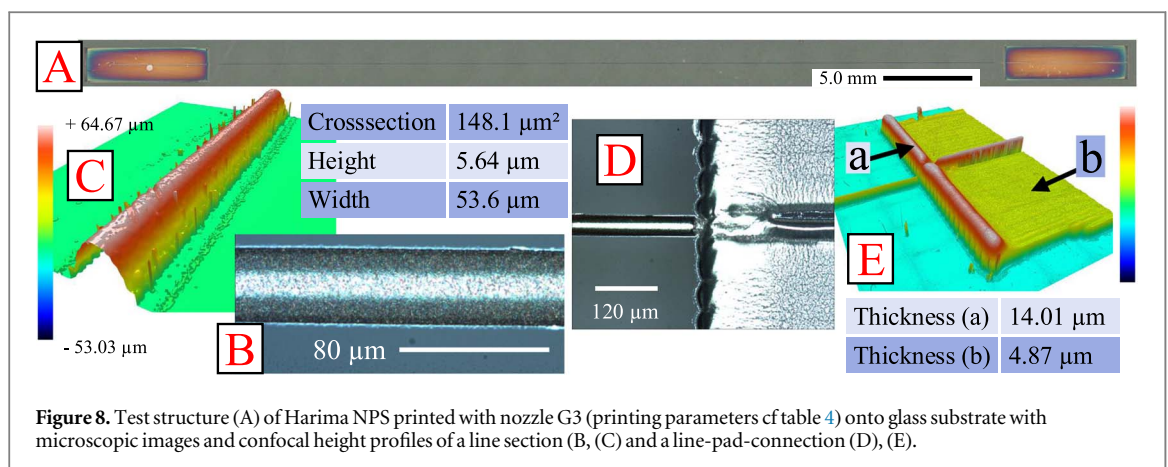
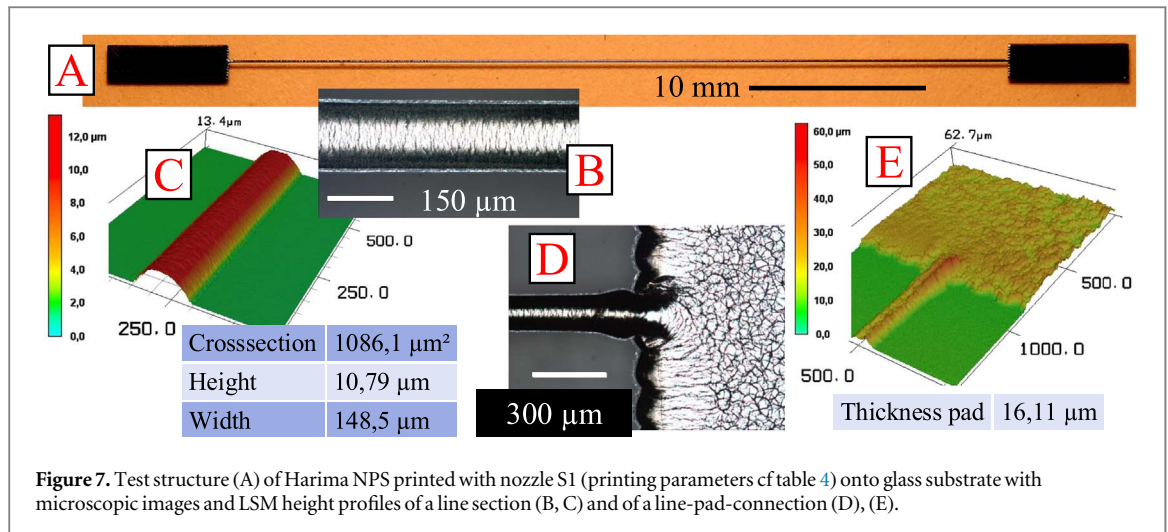
## 2.6. Printing of planar test structures

figure 6 shows a test structure that has been defined as a straight line ( $l_l = 45 \text{ mm}$ ) connecting two contact pads ( $l_p = 7 \text{ mm}$ ,  $w_p = 2 \text{ mm}$ ). The design is created with the objective to have the longest straight line that fits both into an existing tensile test setup [51, 52] and to a four point probe adapter for resistance measurement matched to a substrate size of microscope glass slide format [2, 53].

Based on the previously determined parameter windows for the standard dispensing tips and the glass printing nozzles (see table 3), these planar test structures are printed with the above inks on polyimide and glass substrates following the methodology introduced above. The parameters identified for reproducible printing of the test structures are summarised in table 4.

## 2.7. Characterization methods

Light microscopes from Zeiss and Leica with motorized xy-stage and USB 3.0-camera are used in combination with the image processing software Diplom (developed at IAI) for optical characterization of the line quality and for measurement of the line width.



A confocal laser-scanning-microscope (LSM) Keyence VK-9700 is used for analyzing the topography of the printed structures in combination with the Keyence softwares VK-Analyzer and VK-Viewer. The cross section, the height and the width of printed lines are obtained from measurement data of the LSM.

Some printed lines are additionally analyzed by means of a Sensofar S neox 035 non-contact 3D optical profiler (confocal, interferometry, focus variation).

The resistance of the planar test structures is measured with a Keithley SourceMeter 2612 in combination with a self-built four-point measurement setup. By means of a probing adapter and a sample holder, each pad of the test structure is contacted with two spring-loaded contact pins.

### 3. Results

As depicted in section 2.5 reproducible EP of conductive tracks onto planar substrates is possible. But as can be seen from the parameters of table 4, printing of larger surface areas as required for the contact pads of the test structures takes a lot of time due to the large number of parallel lines needed when using a small nozzle and Harima NPS. Moreover the printing speed is limited as the maximum available pressure is reached for EP of the NPS ink both with standard dispensing tips and small glass nozzles. Due to the size of the silver particles in DYAG50 the application of small glass nozzles and thus smaller structure width is limited; for larger tips the flow behaviour is more favorable and therefore a lower pressure is needed for ink extrusion and hence a higher printing speed is possible. For the described reasons only a few complete planar test structures are printed.

Figures 7, 8 and 9 show results of entire planar test structures printed with Harima NPS with standard dispensing tips and glass nozzles onto glass slides as well as onto Kapton HN films. It can be seen that lines and pads printed with standard dispensing tips show cracks that form during post processing (cf figure 7 (D)). The assumption of crack formation due to drying processes is substantiated by comparing the structure heights with the maximum post cure thickness of 7  $\mu\text{m}$  indicated by Harima for screen printing of NPS. Except for the cracks

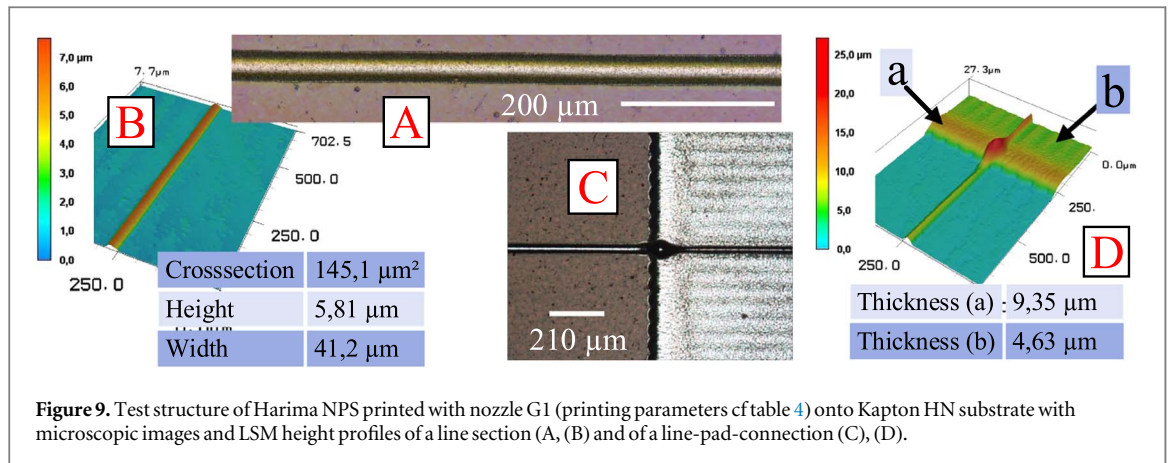


**Figure 9.** Test structure of Harima NPS printed with nozzle G1 (printing parameters cf table 4) onto Kapton HN substrate with microscopic images and LSM height profiles of a line section (A, B) and of a line-pad-connection (C, D).

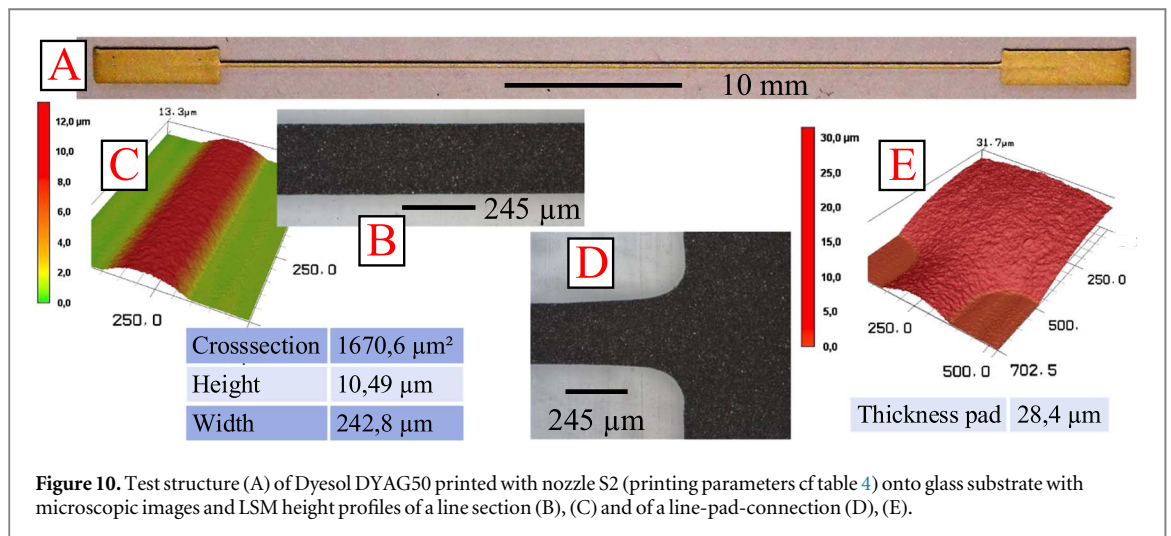


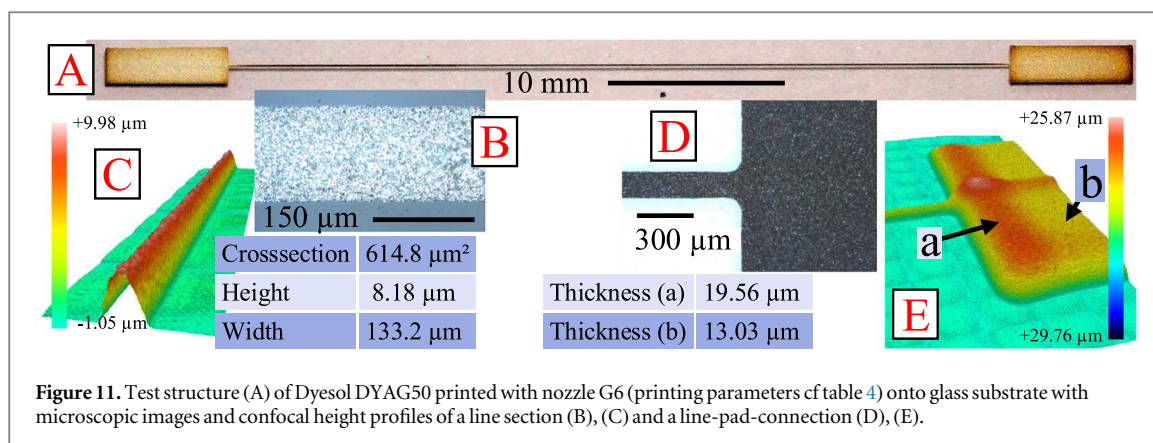
**Figure 10.** Test structure (A) of Dyesol DYAG50 printed with nozzle S2 (printing parameters cf table 4) onto glass substrate with microscopic images and LSM height profiles of a line section (B), (C) and of a line-pad-connection (D), (E).

the lines and pads are of a homogeneous shape. The pads printed with glass nozzles show considerably smaller cracks compared to the ones printed with standard dispensing tips (cf figures 8 (D) and 9 (C)). The lines do not show any crack. Here the aspect ratio of printed lines with NPS is about 0.08 for standard dispensing tips and 0.14 for glass nozzles. We find that the aspect ratio of the printed structures not only depends on the wetting behavior,  $\Delta z$  and the choice of the nozzle but can be controlled by the ratio between the mean flow rate at the orifice and the printing speed. The connections between pads and lines are more critical when using glass nozzles. In that case the narrow line seems to be subjected to a higher drying speed and therefore to lower leveling and nearly no merging with the already printed pads.

The figures 10, and 11 show results of entire planar test structures printed with Dyesol DYAG50 with standard dispensing tips and glass nozzles onto glass slides. Both the structures printed with standard dispensing tips and with glass nozzles are very homogeneous. The connections between lines and pads are well formed and show favorably filleted junctions. The pads printed with standard dispensing tips are not as close to nominal dimensions as the pads printed with the glass nozzle, that show very sharp edges. In contrast to Harima NPS the structures printed with DYAG50 do not show any crack formation. The maximum measured aspect ratio is about 0.065 for standard dispensing tips.

For Harima NPS printed with standard dispensing tips onto glass substrates we achieve a line resistance of 1.30  $\Omega$  (mean value  $\pm$  standard deviation) measured by the four-point-method. Based on the LSM-measurements this yields a resistivity of 3.34  $\mu\Omega\text{cm}$  [53] which corresponds to twice the resistivity of bulk silver at 298 K [54]. On the polyimide substrates the structures printed with standard dispensing nozzles have a resistivity of 3.54  $\mu\Omega\text{cm}$  [53]. The test structures printed with glass nozzles onto glass slides yield a resistivity of about 4.03  $\mu\Omega\text{cm}$  [53] and onto Kapton HN 4.31  $\mu\Omega\text{cm}$  [53].

For Dyesol DYAG50 printed with standard dispensing tips onto glass substrates we achieve a line resistance of 1.90  $\Omega$ . Based on the LSM-measurements this yields a resistivity of 7.06  $\mu\Omega\text{cm}$  [53] which corresponds to about 4.4 times of the resistivity of bulk silver at 298 K. The structure printed with the glass nozzle onto a glass slide has a resistance of 9.57  $\Omega$  [53] and a resistivity of about 13.07  $\mu\Omega\text{cm}$ .



The compared to inkjet printing high thickness of the extrusion printed structures, pointed out in figures 7 to 11, leads not only to significantly lower resistivities but also to higher mechanical robustness. They do not exhibit visible wear or damage after our resistance measurements with springloaded probing pins.

#### 4. Discussion

We have systematically investigated an EP process based on a standard time-pressure dispenser, two commercial screen printing inks, one self developed and two commercial nozzle types. Both theoretical considerations and dispensing experiments confirm that geometric tolerances of the nozzles significantly influence the printing process. The tolerances of the standard and medium quality metal nozzles require inspection and dimensional measurement of the nozzle item being used. Adaptation of EP process parameters derived from these nozzle characterisation data allow good printing results also for such lower quality nozzle types. The investigated glass nozzles exhibit the best quality, smooth inner surfaces and low dimensional tolerances. Thus, they are best suited for EP with high reproducibility down to linewidths below  $20\ \mu\text{m}$ . Nozzle clogging was observed depending on the volumetric ratio of the ink particles, their size and shape and the particle size/nozzle diameter ratio limits as outlined in the literature. However for very small nozzle diameters due the small ink volume and thus an unfavourable surface to volume ratio drying effects at the nozzle outlet seem also to contribute to nozzle clogging. The investigated inks show significantly different rheological properties and wetting behaviours on the used substrates. Process windows defining forward pressure, nozzle standoff distance and nozzle velocity have been identified for different nozzle/ink/substrate combinations. For a given nozzle/ink/substrate/standoff distance/forward pressure combination relations between printing velocity and linewidth have been identified. These allow variation of linewidth by a factor of two by varying printing velocity by a factor of ten. The established process windows have been applied to print planar test structures which subsequently were characterised by optical inspection and four point resistance measurement. The results show high reproducibility with respect to geometrical dimensions and resistance. Moreover due to the increased height of printed structures and the high metal content of the inks very low resistivities down to less than  $4\ \mu\Omega\text{cm}$  can be achieved; significantly lower than e.g. with ink jet printing. Furthermore, sophisticated EP strategies have been derived from the printing experiments. One example is to print narrow line structures with well defined edges with the Harima NPS ink. For two dimensional structures like e.g. pads the smoother wetting behaviour of the Dyesol DYAG50 inks yields more homogeneous surfaces.

#### 5. Conclusion

The investigations presented show that EP with commercial conductive inks with high particle load is indeed a promising process to print highly conductive structures with high resolution. In order to fully exploit its potential, tolerances in ink properties and dimensional tolerances of printing nozzles have to be eliminated as far as possible or at least identified and taken into account by adapting process parameters. Methods to achieve this have been outlined in this paper. There is however room for improvement. As it is a printing process requiring a permanent fluidic bridge between nozzle and substrate, the ink flow and the nozzle standoff distance have to be tightly controlled. With an improved set-up e.g. by application of a time-pressure dispenser with mass flow control or a volumetric dispenser and a closed loop control of the nozzle standoff distance even finer structures with linewidths below  $10\ \mu\text{m}$  can be reproducibly printed on planar substrates. In order to go beyond 2D structures our EP process has been implemented on a four axis plc-controlled motion system. As outlined above

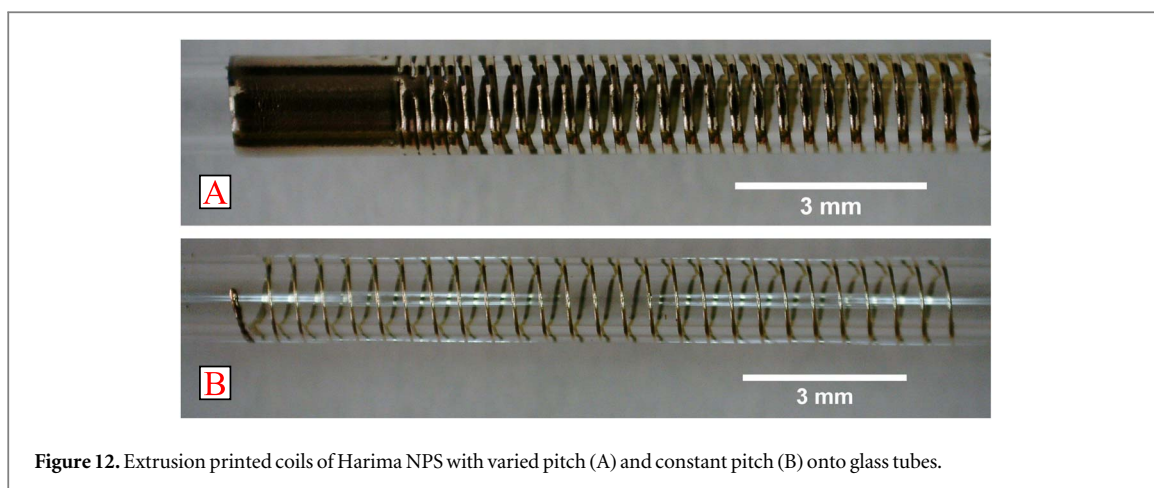


**Figure 12.** Extrusion printed coils of Harima NPS with varied pitch (A) and constant pitch (B) onto glass tubes.

three orthogonal linear axes allow printing of planar structures. A fourth rotational axis has been implemented to clamp and rotate cylindrical substrates. This set-up has been applied to print solenoid coils with varying pitch and number of turns onto glass tubes.

Figure 12 shows two results of first realized test coils on glass tubes. Varying the rotation velocity/feed rate ratio during the printing process allows to realize closed, homogeneous cylinder surfaces (see figure 12 (A) on the left) on the one hand and coils with defined pitches (see figure 12 (A) on the right) on the other hand. In contrast, sample B is printed with a constant ratio and therefore coils with constant pitch can be realized. The first results show potential to print cylindrical coils for various applications such as for nuclear magnetic resonance measurements. These will be outlined in subsequent publications.

## Acknowledgments

This work was funded by the program Materials Systems Engineering of the Helmholtz Association.

The authors would like to thank to B. Hochstein at the KIT-MVM for the rheometer analysis of the Harima NPS ink. Furthermore the authors would like to thank to T. Scharnweber at the KIT-IBG 1 for providing the laser scanning microscope.

## Data availability statement

The data cannot be made publicly available upon publication because they are not available in a format that is sufficiently accessible or reusable by other researchers. The data that support the findings of this study are available upon reasonable request from the authors.

## Contributions

M U conceived the printing process and the experiments. M U and A H conceived the glass printing nozzles. M U and K-M R realized the printing system. J M and V M fabricated glass dispensing nozzles. C D, J M, V M and M U conducted the experiments. M U and U G discussed the results and wrote the manuscript.

## Conflict of interest

The authors declare no conflict of interest.

## ORCID iDs

Martin Ungerer  <https://orcid.org/0009-0000-4026-6338>

## References

- [1] Clemens W, Lupo D, Kirchmeyer S, Hecker K and Ranfeld C 2017 *White Paper: OE-A Roadmap for Organic and Printed Electronics (7th Edition)* OE-A (VDMA) Frankfurt am Main

- [2] Ungerer M 2020 *Neue Methodik zur Optimierung von Druckverfahren für die Herstellung funktionaler Mikrostrukturen und hybrider elektronischer Schaltungen [New methodology for the optimization of printing processes for the fabrication of functional microstructures and hybrid printed electronics]* Ph.D. thesis Karlsruhe Institute of Technology (KIT) Karlsruhe
- [3] Wiklund J, Karakoç A, Palko T, Yiğitler H, Ruttik K, Jäntti R and Paltakari J 2021 A Review on Printed Electronics: Fabrication Methods, Inks, Substrates, Applications and Environmental Impacts *Journal of Manufacturing and Materials Processing* **5** 89
- [4] Khan Y, Thielens A, Muin S, Ting J, Baumbauer C and Arias A C 2020 A New Frontier of Printed Electronics: Flexible Hybrid Electronics *Adv. Mater.* **32** 1905279
- [5] Yan K, Li J, Pan L and Shi Y 2020 Inkjet printing for flexible and wearable electronics *APL Mater.* **8** 120705
- [6] Hecker K and Vertraelen S 2017 *Organic and Printed Electronics: Applications, Technologies and Suppliers (7th Edition)* OE-A (VDMA) (Frankfurt am Main)
- [7] Alamán J, Alicante R, Peña J I and Sánchez-Somolinos C 2016 Inkjet Printing of Functional Materials for Optical and Photonic Applications *Materials* **9** 910
- [8] Medina Rodríguez B 2016 Inkjet and screen printing for electronic applications Ph.D. thesis University of Barcelona Barcelona
- [9] Sridhar A, Blaudeck T and Baumann R R 2011 Inkjet Printing as a Key Enabling Technology for Printed Electronics *Material Matters* **6** 12–15
- [10] Öhlund T, Örtengren J, Forsberg S and Nilsson H E 2012 Paper surfaces for metal nanoparticle inkjet printing *Appl. Surf. Sci.* **259** 731–9
- [11] Tomaszewski G and Potencki J 2017 Drops forming in inkjet printing of flexible electronic circuits *Circuit World* **43** 13–18
- [12] Klug A, Patter P, Popovic K, Blümel A, Sax S, Lenz M, Glushko O, Cordill M J and List-Kratochvil E J W 2015 Recent progress in printed 2/3d electronic devices *Proceedings of SPIE* **9569** 95690N
- [13] Zergioti I 2013 Laser Printing of Organic Electronics and Sensors *Journal of Laser Micro/Nanoengineering (JLMN)* **8** 30–34
- [14] Fernández-Pradas J M, Sopena P, González-Torres S, Arrese J, Cirera A and Serra P 2018 Laser-induced forward transfer for printed electronics applications *Appl. Phys. A* **124** 214
- [15] Raje P V and Murmu N C 2014 A Review on Electrohydrodynamic-inkjet Printing Technology *International Journal of Emerging Technology and Advanced Engineering* **4** 174–1–1–183
- [16] An B W, Kim K, Lee H, Kim S Y, Shim Y, Lee D Y, Song J Y and Park J U 2015 High-Resolution Printing of 3D Structures Using an Electrohydrodynamic Inkjet with Multiple Functional Inks *Adv. Mater.* **27** 4322–8
- [17] Gupta A A, Bolduc A, Cloutier S G and Izquierdo R 2016 Aerosol jet printing for printed electronics rapid prototyping 2016 *IEEE International Symposium on Circuits and Systems (ISCAS) (Montreal, QC, Canada, 22–25 May 2016)* (IEEE) pp 866–9
- [18] Agarwala S, Goh G L and Yeong W Y 2017 Optimizing aerosol jet printing process of silver ink for printed electronics 2nd *International Conference on Mining, Material and Metallurgical Engineering* 191 (Bangkok, Thailand, 17–18 March 2017) (IOP) 012027
- [19] Skarzyński K, Krzemiński J, Jakubowska M and Słoma M 2021 Highly conductive electronics circuits from aerosol jet printed silver inks *Sci. Rep.* **11** 18141
- [20] Seiberlich M, Strobel N, Ruiz-Preciado L A, Ruscello M, Lemmer U and Hernandez-Sosa G 2021 Aerosol-Jet-Printed Donor-Blocking Layer for Organic Photodiodes *Advanced Electronic Materials* **7** 2000811
- [21] Shah M A, Lee D G, Lee B Y and Hur S 2021 Classifications and Applications of Inkjet Printing Technology: A Review *IEEE Access* **9** 140079–140102
- [22] Wang Y, Hong Y, Zhou G, He W, Gao Z, Wang S, Wang C, Chen Y, Weng Z and Wang Y 2019 Compatible Ag+ Complex-Assisted Ultrafine Copper Pattern Deposition on Poly(ethylene terephthalate) Film with Micro Inkjet Printing *ACS Applied Materials & Interfaces* **11** 44811–9
- [23] Cook B, Liu Q, Butler J, Smith K, Shi K, Ewing D, Casper M, Stramel A, Elliot A and Wu J 2018 Heat-Assisted Inkjet Printing of Tungsten Oxide for High-Performance Ultraviolet Photodetectors *ACS Applied Materials & Interfaces* **10** 873–9
- [24] Godlinski D, Zichner R, Zöllmer V and Baumann R R 2017 Printing technologies for the manufacturing of passive microwave components: antennas *IET Microwaves, Antennas & Propagation* **11** 2010–5
- [25] Cordonier G J and Sierros K A 2020 Unconventional Application of Direct Ink Writing: Surface Force-Driven Patterning of Low Viscosity Inks *ACS Applied Materials & Interfaces* **12** 15875–84
- [26] Favez M, Morsi K and Sabry M N 2017 All-ink fabrication of a tips-pentacene otft using plotter printing technique in all-air environment *Intl Conf on Advanced Control Circuits Systems (ACCS) Systems & 2017 Intl Conf on New Paradigms in Electronics & Information Technology (PEIT) (Alexandria, Egypt, 05-08 Nov. 2017)* (IEEE) pp 319–20
- [27] Singaraju S A, Baby T T, Neuper F, Kruk R, Hagmann J A, Hahn H and Breitung B 2019 Development of Fully Printed Electrolyte-Gated Oxide Transistors Using Graphene Passive Structures *ACS Applied Electronic Materials* **1** 1538–44
- [28] Cai L, Zhang S, Miao J, Yu Z and Wang C 2016 Fully Printed Stretchable Thin-Film Transistors and Integrated Logic Circuits *ACS nano* **10** 11459–68
- [29] Hussain N, Fu T, Marques G, Das C, Scherer T, Bog U, Berner L, Wacker I, Schröder R, Aghassi-Hagmann J and Hirtz M 2021 High-Resolution Capillary Printing of Eutectic Gallium Alloys for Printed Electronics *Adv. Mater. Technol.* **6** 2100650
- [30] Lewis J A and Gratson G M 2004 Direct writing in three dimensions *Mater. Today* **7** 32–39
- [31] Wang F, Mao P and He H 2016 Dispensing of high concentration Ag nano-particles ink for ultra-low resistivity paper-based writing electronics *Sci. Rep.* **6** 21398
- [32] Sobolewski P, Goszczyńska A, Aleksandrak M, Urbaś K, Derkowska J, Bartoszewska A, Podolski J, Mijowska E and El Fray M 2017 A biofunctionalizable ink platform composed of catechol-modified chitosan and reduced graphene oxide/platinum nanocomposite *Beilstein J. Nanotechnol.* **8** 1508–14
- [33] Larson B J, Gillmor S D and Lagally M G 2004 Controlled deposition of picoliter amounts of fluid using an ultrasonically driven micropipette *Rev. Sci. Instrum.* **75** 832–6
- [34] Lewis J A, Smay J E, Stuecker J and Cesarano J 2006 Direct Ink Writing of Three-Dimensional Ceramic Structures *J. Am. Ceram. Soc.* **89** 3599–3609
- [35] Ahn B Y, Duoss E B, Motala M J, Guo X, Park S I, Xiong Y, Yoon J, Nuzzo R G, Rogers J A and Lewis J A 2009 Omnidirectional Printing of Flexible, Stretchable, and Spanning Silver Microelectrodes *Science* **323** 1590–3
- [36] Gratson G M, Xu M and Lewis J A 2004 Microperiodic structures: Direct writing of three-dimensional webs *Nature* **428** 386
- [37] Kwon K S, Rahman M K, Phung T H, Hoath S, Jeong S and Kim J S 2020 Review of digital printing technologies for electronic materials *Flex. Print. Electron.* **5** 043003
- [38] Othman N 2005 Entwicklung eines Verfahrens zum präzisen Punkt- und Linienauftrag von hochviskosem Leitkleber mit einem geregelten Mikrodosiersystem Ph.D. thesis University of Stuttgart Stuttgart [https://elib.uni-stuttgart.de/bitstream/11682/4075/1/Diss\\_Othman\\_hs.pdf](https://elib.uni-stuttgart.de/bitstream/11682/4075/1/Diss_Othman_hs.pdf)

- [39] Wright P K, Dornfeld D A, Chen A, Ho C C and Evanc J W 2010 Dispenser printing for prototyping microscale devices *Transactions of NAMRI/SME* **38** 555–61
- [40] Paulsen J A, Renn M, Christenson K and Plourde R 2012 Printing conformal electronics on 3d structures with aerosol jet technology *Future of Instrumentation International Workshop (FIIW 2012) (Gatlinburg, TN, USA, 08-09 October 2012)* (IEEE) pp 1–4
- [41] Adams J J, Duoss E B, Malkowski T F, Motala M J, Ahn B Y, Nuzzo R G, Bernhard J T and Lewis J A 2011 Conformal Printing of Electrically Small Antennas on Three-Dimensional Surfaces *Adv. Mater.* **23** 1335–40
- [42] Can T T T, Nguyen T C and Choi W S 2019 Patterning of High-Viscosity Silver Paste by an Electrohydrodynamic-Jet Printer for Use in TFT Applications *Sci. Rep.* **9** 9180
- [43] Jang Y, Kim J and Byun D 2013 Invisible metal-grid transparent electrode prepared by electrohydrodynamic (EHD) jet printing *J. Phys. D: Appl. Phys.* **46** 155103
- [44] Lysieñ M, Witczak Ł, Wiatrowska A, Fińczyk K, Gadzałińska J, Schneider L, Stręk W, Karpiński M, Kosior Ł, Granek F and Kowalczewski P 2022 High-resolution deposition of conductive and insulating materials at micrometer scale on complex substrates *Sci. Rep.* **12** 9327
- [45] Ahn B Y, Walker S B, Slimmer S C, Russo A, Gupta A, Kranz S, Duoss E B, Malkowski T F and Lewis J A 2011 Planar and Three-Dimensional Printing of Conductive Inks *Journal of Visualized Experiments* **58** e3189
- [46] Niemeier J 08 April 2013 Prozesssicheres und berührungsloses dosieren von lotpaste: Auf den punkt getroffen *Elektronik Produktion + Prüftechnik (EPP)* <https://epp.industrie.de/allgemein/auf-den-punkt-getroffen/>
- [47] Brewin A, Zou L and Hunt C December 2001 *A guide to best practice for electronic materials dispensing Npl report matc(a)82* National Physical Laboratory <https://eprintspublications.npl.co.uk/2382/1/matc82.pdf>
- [48] MacDermid Alpha 2019 Technical bulletin: Alpha cl-78 dispensing solder paste <https://macdermidalpha.com/sites/default/files/2021-09/alpha-cl-78-solder-paste-en-03jan20-tb.pdf>
- [49] MacDermid Alpha 2020 Technical bulletin: Alpha pv-300 dispensing solder paste <https://macdermidalpha.com/sites/default/files/2021-09/alpha-pv-300-solder-paste-en-09mar20-tb.pdf>
- [50] Gaugel T, Bechtel S and Neumann-Rodekirch J 2001 Advanced micro-dispensing system for conductive adhesives *First International IEEE Conference on Polymers and Adhesives in Microelectronics and Photonics. Incorporating POLY, PEP & Adhesives in Electronics (Potsdam, Germany, 21-24 October 2001)* (IEEE) pp 40–45
- [51] Haas T 2014 Mechanische Zuverlässigkeit von gedruckten und gasförmig abgeschiedenen Schichten auf flexiblem Substrat *Ph.D. thesis* Karlsruhe Institute for Technology
- [52] Nickel F, Haas T, Wegner E, Bahro D, Salehin S, Kraft O, A Gruber P and Colsmann A 2014 Mechanically robust, ITO-free, 4.8% efficient, all-solution processed organic solar cells on flexible PET foil *Sol. Energy Mater. Sol. Cells* **130** 317–21
- [53] Ungerer M 02 March 2021 *Methoden, Materialien und Ergebnisse der Entwicklung funktionaler Druckprozesse. Zusätzliche Daten zur Dissertation: Neue Methodik zur Optimierung von Druckverfahren für die Herstellung funktionaler Mikrostrukturen und hybrider elektronischer Schaltungen* Karlsruhe Institute of Technology (KIT) (<https://doi.org/10.5445/IR/1000099352>)
- [54] Electrical resistivity of pure metals Lide D R (ed) 2005 *CRC Handbook of Chemistry and Physics, Internet Version 2005* (FL: CRC Press)